Journal of Cluster Science (2022) 33:123–133
https://doi.org/10.1007/s10876-020-01965-7

ORIGINAL PAPER

Mangifera indica Resin Assisted Synthesis of Nano Silver: Assessing their Photocatalytic Degradation of Methylene Blue, Anticorrosive and Antioxidant Activity

V. Panneerselvi[1] · **K. Shankar**[2] · **P. Muthukrishnan**[2] · **A. Prabhu**[2]

Received: 6 August 2020 / Accepted: 8 December 2020 / Published online: 1 January 2021

Abstract

The current work focusses on the silver nanoparticles (Ag-NPs) that are conveniently green synthesized by *Mangifera indica* gum powder extract. The absorbance is measured by UV–Vis spectrophotometer at a wavelength of 455 nm that represents the Surface Plasmon Resonance of Ag-NPs. Fourier Transform-Infra Red (FT-IR) spectroscopy confirms the functional groups and reaction mechanisms involved in the green synthesis of Ag-NPs. The elemental analysis of Ag-NPs is carried out by Energy dispersive X-ray (EDAX) spectrum and its surface morphology was studied by High resolution transmission electron microscopy (HR-TEM). The average size of Ag-NPs is found to be around 19 nm in diameter. The crystalline nature of the Ag-NPs is investigated by X-ray diffraction (XRD) and Selected area diffraction (SAED). The Ag-NPs shows better antioxidant activity against free radicals such as 2,2-diphenyl-1-picrylhydrazyl (DPPH) and superoxide anion. Ag-NPs effect on reduction mild steel corrosion is examined using non electrochemical methods. It is proved from experimental tests that the inhibition efficiency increases with increased concentrations of Ag-NPs. The photocatalytic activity of the prepared Ag-NPs under visible light irradiation is assessed by the degradation of methylene blue (MB) dye.

Keywords Natural resin · Antioxidant activity · Corrosion inhibitors · FT-IR · Nanocatalyst · Visible light

Introduction

Nanotechnology is innovative, highly hopeful, magnified and almost identical for altered things. New challenges have arisen creating scientific interest and management for effective interdisciplinary relations. The final objective is to fabricate novel materials and systems that customize the needs of engineering and medical applications [1]. The nanomaterials have more physio-chemical properties than the bulk materials of definite compositions. Nanoparticles are used in several applications such as computer chips, insulators, elimination of pollutants, high energy batteries, magnets, sensors and automobiles. Biosynthesis of nanoparticles gains ecological importance because of safety, eco-friendly, cost-effective and uncomplicated synthesis by using plants, seaweed, bacteria, actinomycetes, yeast, algae and fungi [2–5]. Among the different methods of biosynthesis, micro-organism mediated synthesis of nanoparticles is not feasible for production in large scale industries due to the complications in their maintenance. The utilization of various parts of plants and trees in the synthesis of nanoparticles draws attention as it is rapid, eco-friendly, non-pathogenic and economical in providing single step synthesis [6, 7]. The properties of metal nanoparticles are further modified by capping agents like functional groups, antibodies, ligands and drugs [8]. Nowadays the biosynthesized silver nanoparticles play a major role in treatment of many incurable diseases. The reduction of metal ions by the combination of bio-molecules such as alkaloids, amino acids, tannins, phenolics, flavanoids, terpenoids and vitamins proves to be effective in the biological processes [9]. The phytochemicals present

---

✉ K. Shankar
drkshankar@gmail.com

[1] Department of Chemistry, PSG College of Arts and Science, Coimbatore 641014, India

[2] Department of Chemistry, Faculty of Engineering, Karpagam Academy of Higher Education, Coimbatore 641021, India

in different parts of plants and trees act as reducing, capping and stabilizing agents [10]. The silver nanoparticle is one of the most preferable metal nanoparticles due to its efficient catalytic [11], sensor [12], optical [13] and antimicrobial properties [14]. In addition, Ag-NPs are used in the disinfection and coating of medical instruments, dental substances, historical paper conservation against deteriorated fungi, chemical analysis, electronics, photocatalysis and bone cement [15–17]. Ag-NPs are also used in widely in variety of industries, such as medicals, food-packaging firms, cosmetics, and other industries [17]. Ag-NPs also exert multifunctional broad-spectrum effects with promising therapeutic efficiency in the treatment of burns, open wounds and a number of infections. In addition, silver has been suggested as an antimicrobial agent among other metals, and can be used both in vivo and in vitro studies [18, 19]. *Mangifera indica* also known as mango, consists of different phytoconstituents such as polyphenolics, flavonoids, triterpenoids. The *Mangifera indica* gum is an amber coloured resin which is soluble in water.

Waste water treatment and corrosion control are the most important tasks at various industrial processes like leather tanning, electroplating, mining, leaching, smelting, battery manufacturing, pickling, descaling etc. Every day, many toxic organic pollutants are released from different industries into the environment [20, 21]. Organic dyes play a crucial role in textile, paper and printing industries and so they are always in great demand. Methylene blue (MB) is an organic heterocyclic dye, widely used in cosmetic, pharmaceutical and clothing industries. The molecular structure of methylene blue is shown in Fig. 1. Methylene blue can cause permanent inhalation and ingestion damage to humans and animals and the presence of this colour in water causes burning of eyes, vomiting, diarrhoea and nausea [22]. Ag-NPs have been extensively researched to remove the different dye effluents [23, 24]. In recent years, various forms of natural and organic products have received considerable attention in the presence of acidic media as useful and effective metallic corrosion inhibitors [25–29]. And this study may be the first study on the protection of metal from corrosion and photocatalytic degradation of methylene blue using biosynthesised Ag-NPs as a new effective catalyst.

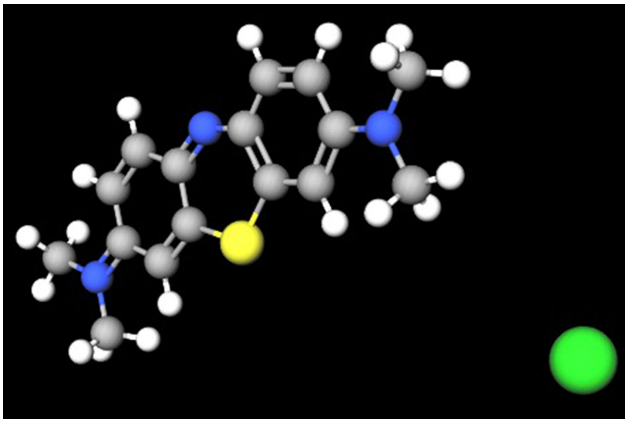

Fig. 1 3D Chemical structure of methylene blue (Color figure online)

In the present study, the facile synthesis of silver nanoparticles (Ag-NPs) is carried out with *Mangifera indica* gum (MIG) powder by the eco-friendly method. The synthesized Ag-NPs is characterized and evaluated for its antioxidant, anticorrosion activities and photodegradation of methylene blue solution. The deciding factors such as contact time, and catalyst dosage influencing the photodegradation are analysed in detail. In addition, the reusability of Ag-NPs to photodegradation of methylene blue is also reached.

Materials and Methods

Preparation of *Mangifera indica* Gum (MIG) Powder Extract

Extracted from the cracks made in a particular portion of the *Mangifera indica* trees found in the Namamalai Hills, of Salem district, Tamil Nadu, the *Mangifera indica* gum is dried well, powdered and passed through mesh no:100. An approximate quantity of 20 g MI gum is added to 100 ml of distilled water for 8 h and stirred well. Through centrifugation method, supernatant is obtained. Washed many times with distilled water, the residue is added to separate the supernatant liquid. About 100 ml of supernatant liquid is treated with 200 ml of acetone and the precipitate obtained is washed using distilled water and dried at 50–60 °C under vacuum. Then it is ground and stored in an airtight container. About 5 g of MIG powder is heated in 100 ml of double distilled water for one hour at 80 °C and cooled to room temperature. The extract is filtered through Whatman No.1 filter paper and the filtrate is stored in a container at 4 °C for further analysis.

Green Synthesis of Ag-NPs by *Mangifera indica* gum (MIG) Powder Extract

In order to synthesise silver nanoparticles, about 10 ml of MIG powder extract is added to 90 ml of 1 mm $AgNO_3$ solution in a 250 ml Erlenmeyer flask at room temperature for 30 min with constant stirring. The colour change from pale yellow to dark brown indicates the formation of Ag-NPs.

Characterization of Ag-NPs

The UV–Visible spectrum of Ag-NPs is evidenced by UV 2450 Shimadzu spectrometer at the range of 200–800 nm wavelength. The functional groups involved in the biosynthesis of Ag-NPs are recognized by FTIR Shimadzu 8400S, Japan in the range of 4000- 400 cm^{-1}. The surface morphology of Ag-NPs is studied using High-Resolution Transmission Electron Microscopy (JEOL JEM 2100, Japan) and the microscope enables the view of lattice resolution of 0.14 nm and point-to-point resolution of 0.19 nm at 200 kV acceleration voltages. HR-TEM is equipped with Gatan Orious CCD camera (2 K × 2 K) for image recording. The diameter of biosynthesized Ag-NPs in HR-TEM image is measured using the image J software. HR-TEM analysis is converted into SAED by simply converting microscopic mode to diffraction mode. The crystallinity of Ag-NPs is identified by X-Ray Diffraction pattern (Shimadzu PW-6000 X-ray Diffractometer).

In vitro Antioxidant Assay

DPPH Radical Scavenging Activity

The DPPH radical scavenging activity is carried out by a slightly modified method [30]. The different concentrations from 1.25 to 20 μg/ml of biosynthesized Ag-NPs and vitamin-C are taken in different test tubes and mixed with 1 ml of 0.1 mM DPPH solution. The above reaction mixture is incubated at room temperature for 30 min. The degree of absorbance is recorded spectrophotometrically at 517 nm. The free radical activity of biosynthesized silver nanoparticles is evaluated using the relationship (1).

$$\text{Scavenging activity (\%)} = \frac{\text{Absorbance of Control (Ac) - Absorbance of test sample (As)}}{\text{Absorbance of Control (Ac)}} \times 100 \qquad (1)$$

Superoxide Anion Scavenging Activity

The superoxide anion radical scavenging activity of Ag-NPs is measured using vitamin-C as the standard [31]. The non-enzymatic phenazine methosulphate/Nicotinamide adenine dinucleotide system generates superoxide anion radicals, which reduces nitro blue tetrazolium to purple diformazan. Different concentrations of Ag-NPs from 12.5 to 200 μg/ml of test sample are prepared and added to the mixture of 1 ml NBT and 1 ml NADH. Then 0.1 ml of PMS is added to the above mixture and incubated in dark at 25 °C for 5 min. Finally, the absorbance is measured at 560 nm. The activity is calculated using relationship (1).

Evaluation of Corrosion Inhibition of MIG Mediated Ag-NPS

Weight loss test was conducted with and without MIG mediated Ag-NPs in a glass beaker containing 100 ml 1 M H_2SO_4 solution. Weight loss measurements were performed as per ASTM standard described previously [32, 33]. Small polished steel square specimens (2.5 × 2.5 × 0.4 cm) with weight percentage composition are used: C = 0.05%, Mn = 0.6%, and P = 0.36% and Si = 0.03% and Fe = 98.96%. Pre-weighted and smooth mild steel specimens are immersed in 100 ml 1 M H_2SO_4 solution with and without Ag-NPs concentrations ranging from 5 to 25 ppm. The test solution temperature is held at 308 K for 2 h. In the next stage, the specimens are taken away from the test solution and washed with deionized water. Once it is dried, it is weighed carefully. This procedure is carried out thrice to ascertain the reproducibility of the weight loss data. The weight loss (ΔW) is used to calculate the corrosion rate (CR) and inhibition efficiency (IE) for each concentrations [34].

$$\mathrm{CR\ (mpy)} = 534 \times W_b - W_a/\mathrm{DST} \qquad (2)$$

$$\mathrm{IE\%} = (W_0 - Wi) / W_0 \times 100 \qquad (3)$$

where W_b and W_a are the specimen weights before and after immersion in the tested solutions. W_0 and Wi refer to the weight loss of mild steel in the absence and presence of Ag-NPs respectively, D is the density of mild steel (7.8 g cm^{-3}), S is the area of the specimen, T is the period of immersion in hours.

Photocatalytic Degradation of Methylene Blue Dye

The degradation efficiency of the Ag-NPs has been tested against aqueous solution of methylene blue dye under visible light irradiation. 40 mg of the Ag-NPs is mixed with 75 ml of (10 mg/l) of methylene blue dye solution in a 100 ml beaker. Then the reaction vessel is held under the irradiation of visible light. Using UV–Visible spectrophotometer, 5 ml of aliquots are obtained by filtration at various time intervals and analysed. The suspensions are agitated magnetically for 1 h in darkness before exposing to visible light to ensure the adsorption–desorption equilibrium of the working solution. The degradation rate of methylene blue dye is calculated using the following equation.

$$\text{Degradation rate } (\%) = (I_0 - I/\ I_0) \times 100 \qquad (4)$$

Here, I_o is the absorption intensity of initial dye solution and I is the main absorption peak intensity of methylene blue.

Statistical Analysis

Statistical analysis of the variance data obtained is carried out using Origin 8.5 software by one-way ANOVA and the Tukey post-test. Differences are considered statistically relevant at $p < 0.05$. Group sizes are indicated in the figure legends. The mean ± SD is expressed in all values.

Results and Discussion

Formation and Confirmation of Ag-NPs Through Various Spectral Analysis

The *Mangifera indica* gum powder extract converts $AgNO_3$ to silver nanoparticles indicating colour changes from yellow to dark brown. The MIG extract does not show any colour change in absence of $AgNO_3$ [35]. The colour change is due to surface Plasmon resonance band observed at 455 nm in the UV–Visible spectrometer (Fig. 2). The SPR band is due to shape, size and surface charge of Ag-NPs formed [36]. Then the biosynthesized Ag-NPs are separated by centrifugation at 15,000 rpm for 30 min and the pellets are re-dispersed in de-ionized water. The maximum absorption peak at a wavelength from 250 to 700 nm in the UV–Vis spectroscopic study was observed at 455 nm (Fig. 2), which may be due to efficient synthesis of spherical Ag-NPs [37]. The standard peak of green synthesized Ag-NPs was observed at 455 nm, which can be attributed to mangiferin involved in biomass filtrate, which convert nitrate (NO_3^-) to nitrite (NO_2^-) and then, the electrons reduced silver ion (Ag +) to metallic silver (Ag^0) and also possess stabilizing, capping, and reducing activities. The FT-IR spectrum (Fig. 3) of MIG extract shows peaks at 3587, 2924, 2854, 1743, 1242 and 972 cm^{-1} corresponding to O–H stretching vibrations (phenolic group), C–H stretching (alkanes), C=O stretching (asymmetric), C–N stretching (aliphatic amines) and C–H (out of plane) [38]. After bio-reduction, the FT-IR peak intensity decreases and new peak appears at 752 cm^{-1} and it may be endorsed to the reduction of Ag^+ ions to Ag^o nanoparticles. It is suggested that phytochemicals such as mangiferin present in M*angifera indica* can also be responsible for biosynthesis of Ag-NPs (Fig. 4).

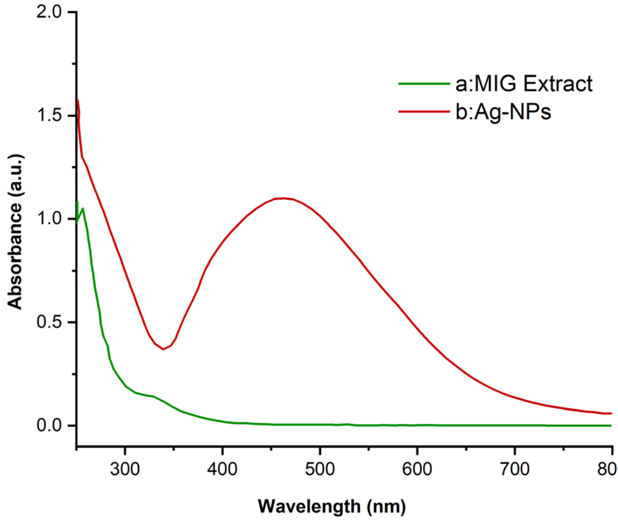

Fig. 2 UV–Visible spectrum of MIG extract and Ag-NPs

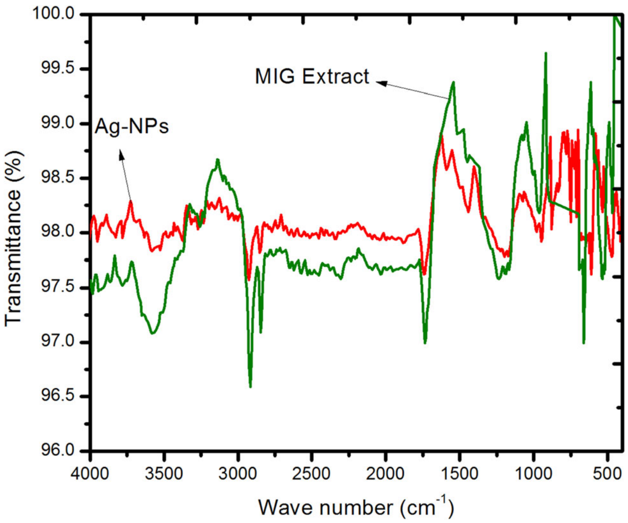

Fig. 3 FT-IR spectrum of MIG extract and Ag-NPs

Based on FT-IR data, the tautomeric conversion of mangiferin from enol to keto liberate reactive hydrogen atoms that reduce silver ions to silver nanoparticles. In XRD pattern (Fig. 5) five peaks appear at different positions (2θ) 38.04°, 44.24°, 64.34°, 77.3° and 81.26° which correspond to (111), (200), (220), (311) and (222). Braggs reflection planes of silver is observed and compared with JCPDS card no. 04-0783 [39]. The XRD pattern confirms that silver has the Face-Centred Cubic lattice structure. Likewise, green synthesized fcc crystallographic structure of Ag-NPs at diffraction peaks (111), (200), (220) and (311) which good agreement with Fouda et al. [40] and Mohmed et al. [41]. The sharp diffraction peaks confirm

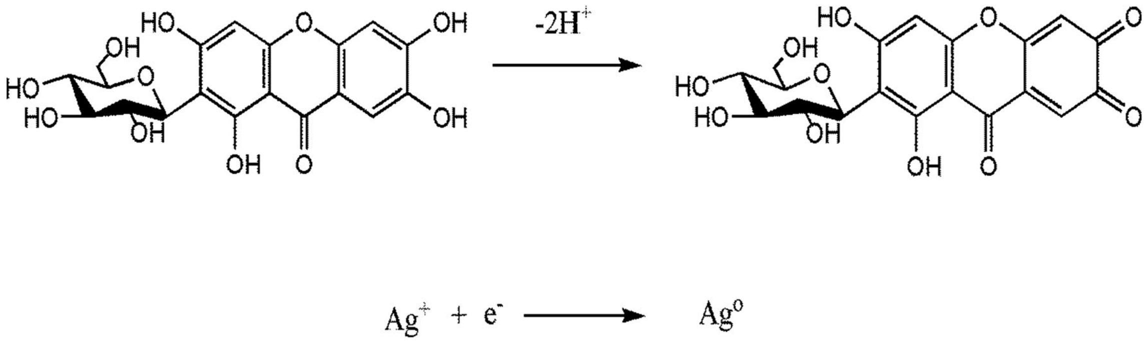

Fig. 4 Plausible mechanism of biosynthesis of Ag-NPs by MIG extract

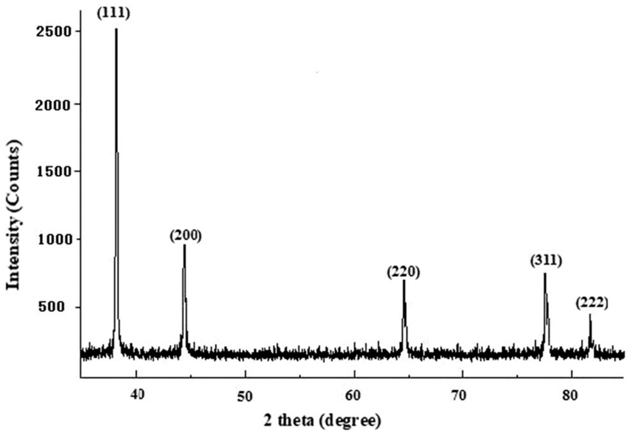

Fig. 5 XRD analysis of Ag-NPs

that low crystallite size of nanoparticles. The average crystallite size of Ag-NPs is calculated by Debye–Scherrer equation as 17.6 nm. The crystallinity index I_{cry} of sample is calculated as 1.07. The I_{cry} value is slightly greater than 1 and it is assumed that low crystallinity index denotes monocrystalline nature of silver nanoparticles.

The HR-TEM image (Fig. 6a) shows the particle is spherical in shape with uniform distribution of Ag-NPs. The calculated average size of Ag-NPs is found to be 19 nm as per Image J 1.51r. The distributed nanoparticles are polydispersed and spherical in shape. The HR-TEM images show small particles aggregates by the capping of organic moiety from plant extracts. The histogram represents the distribution of nanoparticles of different size in the HR-TEM images. Maximum number of particles are noticed between 14 and 20 nm in diameter (Fig. 6b). The bright circular rings in SAED pattern confirm the crystallinity of Ag-NPs (Fig. 6c).

The bright concentric circles indexed at (111), (200), (220) and (311) Bragg reflection planes are good evidence for crystallinity of silver nanoparticles and d-spacing estimated to be 0.22 nm correlates with the orientation of Face Centered Cubic (FCC) structure similar to metallic silver (JCPDS card no. 04-00,783). The elemental analysis of EDAX spectrum (Fig. 6d) shows a strong signal of silver at 3 keV [42]. The percentage of silver (about 83%) represents the purity of Ag-NPs. The appearance of weak oxygen signal in the EDAX spectrum is due to capping of biomolecules on Ag-NPs. The proportion of oxygen is too low when compared with Ag-NPs.

In vitro Antioxidant Studies

The Ag-NPs have the capacity to donate hydrogen or electrons to the free radicals [43]. DPPH radicals can capture electrons or hydrogen from Ag-NPs. Figure 7a shows the DPPH radical scavenging activity of Ag-NPs at different concentrations using 1, 1-diphenyl 1–2-picryl-hydrazyl free radicals. The colour change from purple to yellow indicates the formation of DPPH-H [44]. The DPPH radical scavenging activity is due to the capped organic molecules around the Ag-NPs. The results obtained from the present study show that antioxidant activity increases with increase in the concentrations of Ag-NPs and the maximum free radical scavenging activity of Ag-NPs are against DPPH of 53% at 20 µg/ml respectively. But the standard vitamin-C exhibits 86% at the same concentrations. Likewise, at low concentrations (1.25 µg/ml) biosynthesized Ag-NPs exhibit 16%, which is better than the previous studies carried out by Kumar et al. [45].

The superoxide anion radical is highly reactive and plays an important role in the formation of other free radicals such as hydrogen peroxide and hydroxyl radicals [46]. Superoxide anion radical is known to be harmful for cellular components such as DNA and proteins. Superoxide anion radical scavenging activity of Ag-NPs and vitamin-C are shown in (Fig. 7b). The concentrations of Ag-NPs against superoxide and vitamin-C are increased from 12.5 to 200 µg/ml. The synthesized AgNPs scavenges superoxide anion radicals and inhibit diformazan in a dose dependant manner.

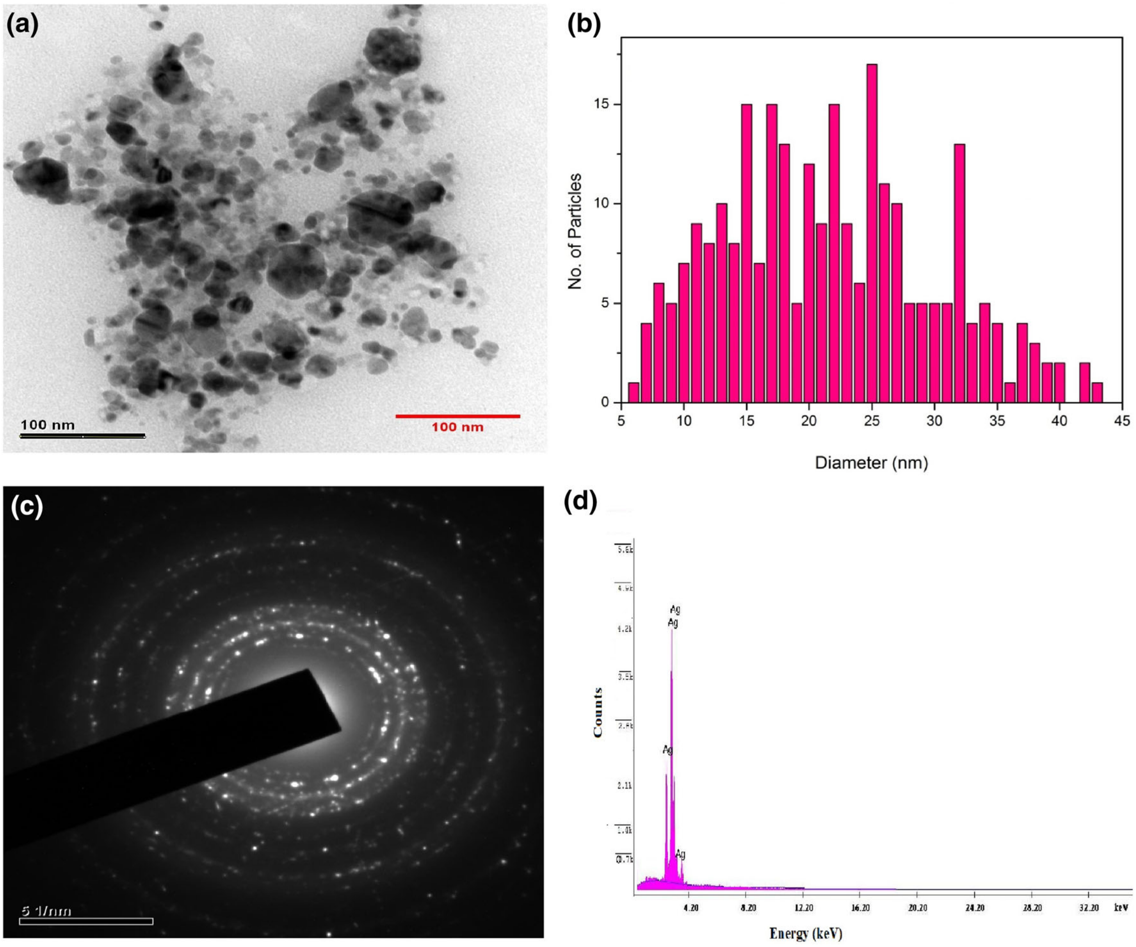

Fig. 6 **a** TEM image of Ag-NPs at 100 nm, **b** size distribution of Ag-NPs, **c** SAED pattern of Ag-NPs, **d** EDAX analysis of Ag-NPs

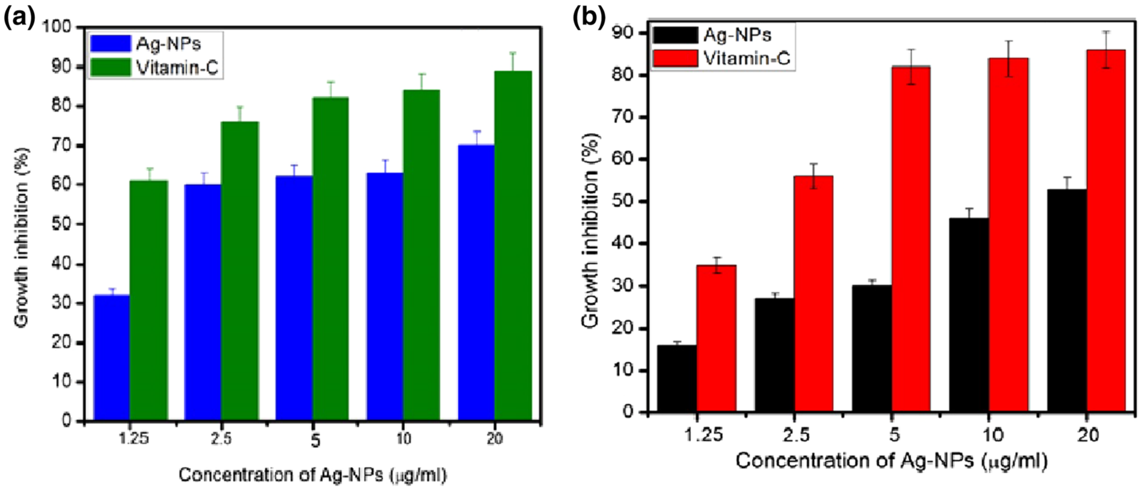

Fig. 7 Antioxidant efficiency of Ag-NPs using DPPH radical (**a**) and Superoxide anion (**b**) scavenging assay

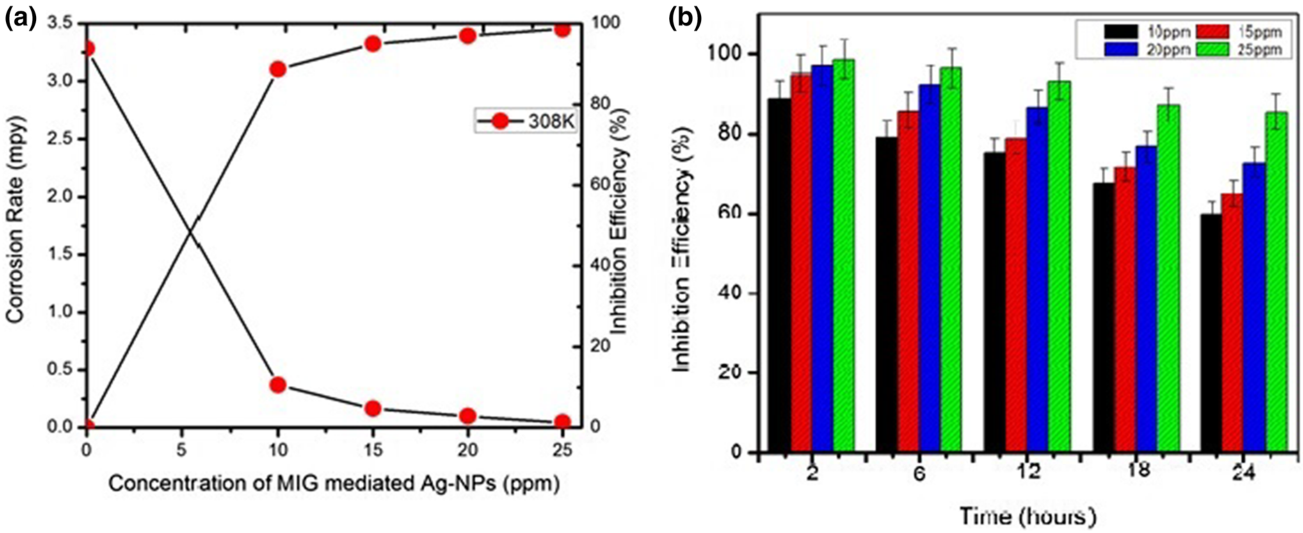

Fig. 8 **a** Effect of Ag-NPs concentrations against CR and % IE, **b** variation of % IE with different exposure time

Potential of Biosynthesized Ag-NPs in Anticorrosive activities

Figure 8a exhibits the effect of MIG mediated Ag-NPs on corrosion rate of mild steel in 1 M H_2SO_4 at 308 K. The figure explains that once the concentrations of MIG mediated Ag-NPs are increased from 5 to 25 ppm, the corrosion. It further states that on a mild steel surface, more MIG mediated Ag-NPs are adsorbed prompting a barrier of insoluble precipitates on the surface of the mild steel. This facilitates protection from the acidic environment inhibiting the corrosion reaction. The maximum performance of this process is formed to be 98.23% at 308 K (25 ppm). It is also observed that further extension of MIG mediated Ag-NPs concentrations do not alter the inhibition result considerably. The reason for the higher protection efficiencies of the MIG mediated Ag-NPs towards mild steel is attributed to the presence of magniferin/AgNPs composite.

In order to assess the stability factor of the inhibitor behaviour “the immersion time” is considered as an important parameter. The inhibition performance deviation known as one of the functions during the exposure priod (2,6,12,18 and 24) for the corrision of mild steel in 1 M H_2SO_4 in the absence and presence of various MIG mediated Ag-NPs concentrations at 308 K.

From the Fig. 8b, it is observed that the efficiency of MIG mediated Ag-NPs inhibition decreases with an increase in the period of exposure time. The inhibition efficiency increases with an increase in the concentrations of MIG mediated Ag-NPs which indicates that MIG mediated Ag-NPs retard the dissolution of mild steel in 1 M $H_2SO_{4.}$ The inhibiting effect of MIG mediated Ag-NPs can be attributed to the adsorption of phytochemicals mediated silver nanoparticle on mild steel surface. Mostly oxygen and nitrogen phytochemicals are responsible for the adsorption. Table 1 shows the percentage of inhibition efficiency for certain nanoparticles used as inhibitors in different corrosive media. The evidence from various nanoparticles and the findings of this research indicate that the MIG mediated Ag-NPs could serve as effective inhibitors.

Degradation Ability of Ag-NPs

The photocatalytic activity of the Ag-NPs is preformed against aqueous solution of methylene blue dye under visible light irradiation. The photo degradation behaviour is described as shown in Fig. 9a with the strong absorption behaviour at 664 nm with 10 mg of aqueous dye solution. On exposure to visible light in the presence of synthesised Ag-NPs, with increased exposure time, the absorption intensity decreases and the intensity reaches almost zero after 75 min which clearly indicates the complete degradation of methylene blue dye under visible light. Hence, synthesised Ag-NPs degrade methylene blue dye in aqueous solution.

One of the important parameters used to evaluate ineffective overload of catalyst is the mass of catalyst loading [57]. The photo degradation efficiency of methylene blue in the presence of different weight of *Mangifera indica* gum mediate Ag-NPs as shown in Fig. 9b. It is seen from the figure that the efficiency of photodegradation increased from 63 to 94% (10 mg/l to 40 mg/l). It is stated that the number of active sites on the Ag-NPs surface increases as the catalyst dosage increases, thus raising the number of O_2^- and OH^- radicals. At 40 mg/l (optimum dosage), the maximum photodegradation methylene blue by Ag-NPs (94%) is noticed. Further increase of dosage of Ag-NPs

Table 1 Inhibition efficiencies of various nanoparticles on metal in various corrosive media

Nanoparticles	Metal exposed	Test solution	Corrosion measurement techniques	Highest inhibition efficiency (%)	Refs.
Polydopamine (PDA)	Mild steel	1 M HCl	Weight loss	86.42	[47]
MgO and epoxy	Mild steel	3.5% NaCl	Weight loss	93.70	[48]
Ag and Poly (ethylene glycol)thiol	Carbon steel	M HCl	Potentiodynamic polarization and EIS	90.95	[49]
CuO	Copper	3.5% NaCl	Potentiodynamic polarization	86.2	[50]
Magnetic nanofluid	Carbon steel	1 M H_2SO_4	Weight loss and potentiodynamic polarization	75	[51]
Mn_2O_3	Carbon steel	0.5 M HCl	Potentiodynamic polarization and EIS	23–56	[52]
Ag-NPs	Mild steel	0.5 M HCl	Potentiodynamic polarization & EIS	91.60 93.10	[53]
Ag-NPs	Mild steel	0.5 M HCl	Potentiodynamic polarization	78.31	[54]
Ag-NPs	Mild steel	Cooling water	Weight loss	77.00 91.70	[55]
Ag-NPs	Mild steel	15% H_2SO_4 15% HCl	Weight loss	88.86	[56]
Ag-NPs	Mild steel	1 M H_2SO_4	Weight loss	98.23	In this work

does not improve the photo degradation efficiency. The constant efficiency above 40 mg describes competition for adsorption of methylene blue by Ag-NPs (which in 40 mg of Ag-NPs is completely covered by methylene blue) and/or return of adsorbed dye molecules to the aqueous solution.

The stability and reusability of the catalyst is a significant parameter for its practical applications. Furthermore, additional experiments are performed for the photo degradation of methylene blue over Ag-NPs under visible light irradiation and the results are shown in Fig. 9c. It shows that Ag-NPs have excellent stability and recycling performances even after 5 days. For five successive Ag-NPs cycling, the percentage of methylene blue photo degradation is 93%, 91%, 90%, 90% and 89% respectively. There is no clear decrease in photo catalytic activity after 5 cycles. The findings show better photo catalytic activity of Ag-NPs for degradation of cationic methylene blue dyes in aqueous solution. The degradability of biosynthesized Ag-NPs is compared with the various synthesized doped Ag-NPs as shown in Table 2.

In optic to get more information about the involvement of primary active species in the degradation of Methylene blue solution, control experiments with the addition of potassium persulfate, ammonium oxalate, acryl amide and tert-butanol as a scavengers for electrons (e^-), holes (h^+), superoxide radicals ($O_2^{\cdot -}$) and hydroxyl radicals (OH*) were performed. The photodegradation efficiency was approximately 96% in the absence of scavengers. Whereas, when using the scavengers, a slight change in the degradation rate was observed. When using the acryl amide as the singlet oxygen quencher, the rate of photodegradation was suppressed which suggests the active involvement of $\dot{O_2}^{-}$. The OH* radical scavenger, t-BuOH generally decrease the rate of the photocatalytic reaction, mainly proceeded by the OH*. In the present study, it was observed that the enormous decrease in the rate of photocatalytic reaction in the presence of acryl amide which clearly showed that the active involvement of $O_2^{\cdot -}$ in the reaction. Furthermore, the addition of ammonium oxalate and potassium persulfate slightly retarded the photodegradation efficiency. Hence, the findings suggested that both $O_2^{\cdot -}$and OH* play a significant dynamic role, while e^- plays a minor role in the successful degradation of MB.

Mechanism of Methylene Blue Degradation

The photocatalytic operation mainly involves light absorption, generation and electron–hole pair transport. For an effective photocatalytic action, the concentration, surface energy, surface area and contact angle with the dye and photocatalyst are very important parameters. To clarify the enhanced photocatalytic behaviour of Ag-NPs, a potential mechanism is proposed [Fig. 10 and Eqs. (5, 6, 7, 8 and 9)]. Ag-NPs absorb the photons when irradiated by visible light and subsequently produce an electron–hole pair due to their powerful Surface Plasmon Resonance (SPR) effect. The produced electrons (e^-) and

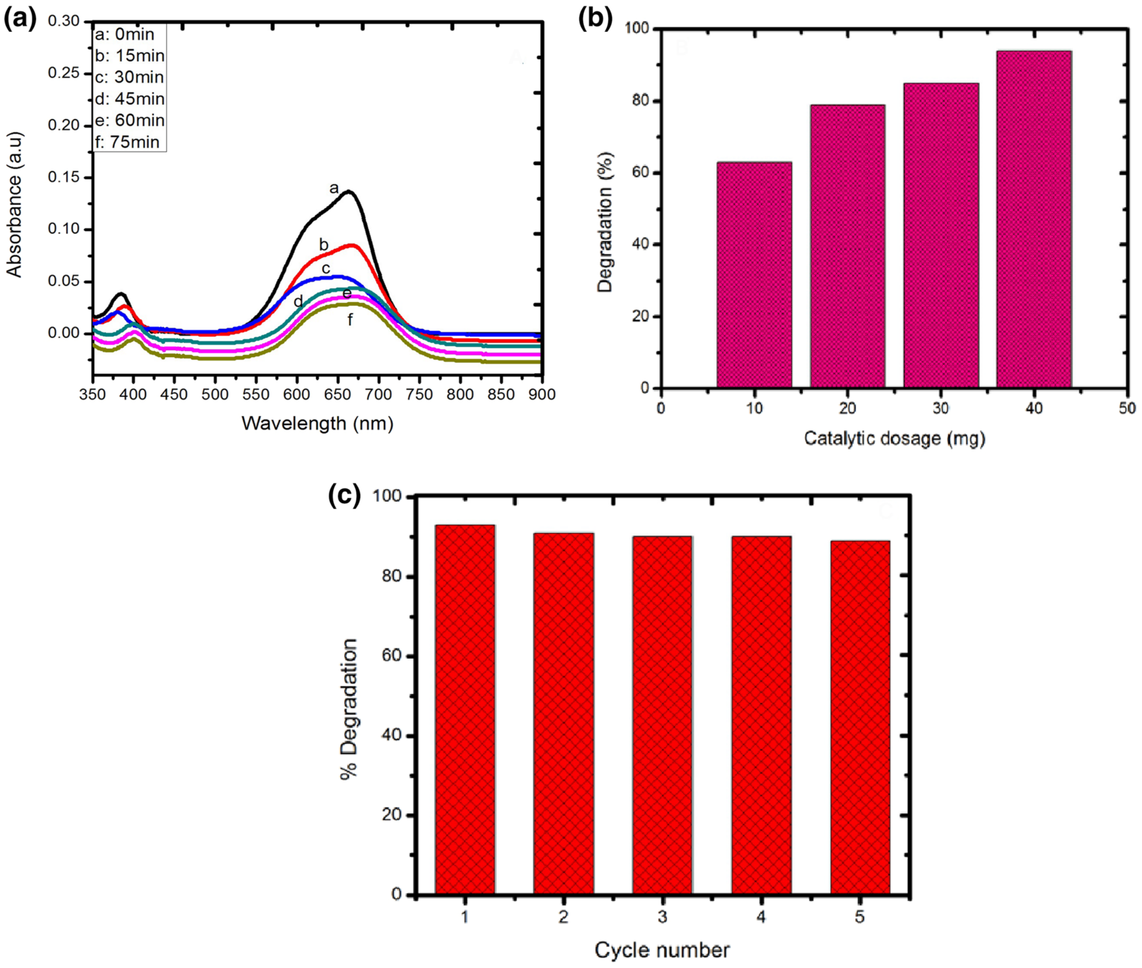

Fig. 9 UV spectrum of photodegradation of Methylene blue dye, **a** different time intervals, **b** effect of catalytic dosage, **c** recycle ability of Ag-NPs

Table 2 Comparison of degradation capabilities of different biosynthesized Ag-NPs against various water pollutants

Source	Nano catalyst	Time (min)	Water pollutants	Light source	Percentage degradation (%)	Refs.
Cynodon dactylon (L.) Pers. Leaf extracts	Ag-NPs	7200	Methylene blue	Sun light irradiation	75	[58]
Imperata cylindrica extracts	Ag -NPs	14	Methylene blue	Visible irradiation	92	[59]
Prosopis farcta fruit extract	Ag -NPs	250	Methylene blue	isible irradiation	86.38	[60]
Pomegranate Peel extracts	Ag-NPs	4320	Methylene blue	Sun light irradiation	89	[61]
Camellia sinensis leaf extract	Ag-NPs	60	Methylene blue	Visible irradiation	65	[62]
Hydrocotyle asiatica Leaf extracts	Ag-NPs	120	Methylene blue	Sun light irradiation	90	[63]
Mangifera indica gum powder extract	Ag-NPs	75	Methylene blue	Visible irradiation	94	In the present study

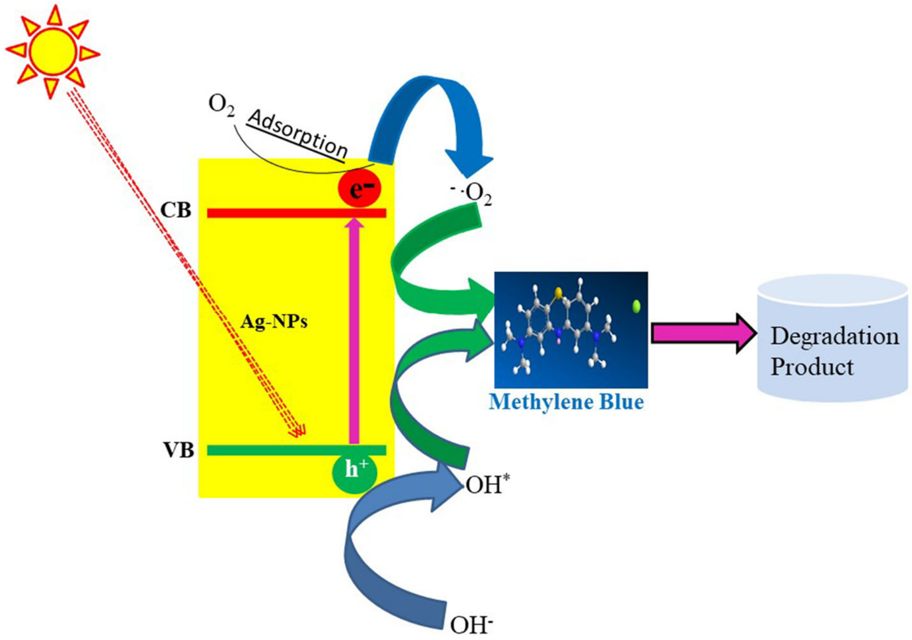

Fig. 10 Photodegradation route of methylene blue in the presence of Ag-NPs under Visible light

hole (h^+) reacts with oxygen and water, creating the reactive species of superoxide radical anions ($O_2^{\,-}$) and hydroxyl radicals (OH*) and these radicals will convert the MB molecules into products, which are colourless. In addition, electron donation from Ag-NPs to MB, results in the decrease of the intensity of the MB absorption peak. The results of the work presented here show that the synthesized Ag-NPs exhibit excellent ability to destroy MB dye, suggesting that the Ag-NPs properties have a powerful influence on their behaviour.

$$\mathrm{Ag} + \text{Visible light} \rightarrow \mathrm{Ag} + h^+_{VB} + e^-_{CB} \tag{5}$$

$$e^-_{CB} + O_2 \rightarrow {}^{-\cdot}O_2 \tag{6}$$

$${}^{-\cdot}O_2 + H_2O \rightarrow HO_2^* + OH^* \tag{7}$$

$$HO_2^* + H_2O \rightarrow H_2O_2 + OH^* \tag{8}$$

$$h^+_{VB} + OH^* + MB \rightarrow \text{Degradation products} \tag{9}$$

Conclusion

The biosynthesized silver nanoparticles (Ag-NPs) are synthesized using *Mangifera indica* gum powder. It is an economical, rapid, convenient and eco-friendly method in the synthesis of Ag-NPs. The biosynthesized Ag-NPs is characterized by UV–Vis, FT-IR, XRD, SAED and EDAX spectrum. The structure of Ag-NPs is Face-Centered Cubic with an average crystallite size of 17.6 nm in diameter. The HR-TEM images show the spherical shape of Ag-NPs with an average size of 19 nm in diameter. The biosynthesized Ag-NPs show good antioxidant activity against free radicals. MIG mediated Ag-NPs is a novel effective corrosion inhibitor for mild steel in 1 M H_2SO_4 at 308 K. The inhibition efficiency enhances with an increase in the concentrations of MIG mediated Ag-NPs but decreases slightly with an increase in immersion time. The maximum photocatalytic behaviour of Ag-NPs is due to an increase in the efficiency of charge separation and extension of wavelength to the visible region. Ag-NPs can be reused five times without a significant drop in their activity.

References

1. S. Prabhu and E. K. Poulose (2012). *Int. Nano. Lett.* **2**, 32.
2. A. Ingle, A. Gade, S. Pierrat, C. Sonnichsen, and M. K. Rai (2008). *Curr. Nanosci.* **4**, 141.
3. P. Rajasekar, S. Palanisamy, R. Anjali, M. Vinosha, M. Thillaieswari, B. Malaikozhundan, P. Boomi, M. Saravanan, S. G. You, and N. M. Prabhu (2020). *J. Clust. Sci.* **31**, 673.
4. M. Gomathi, A. Prakasam, and P. V. Rajkumar (2019). *J. Clust. Sci.* **30**, 995.
5. H. Fouad, L. Hongjie, D. Yanmei, Y. Baoting, A. El-Shakh, G. Abbas, and M. Jianchu (2016). *Artif. Cells Nanomed. Biotechnol.* **45**, 1369.
6. A. Prabhu, K. Shankar, P. Muthukrishnan, and K. Prabhakaran (2015). *Int. J. Pharm. Biol. Sci.* **6**, 423.
7. R. Madhankumar, P. Sivasankar, D. Kalaimurugan, and S. Murugesan (2020). *J. Clust. Sci.* **31**, 719.
8. P. Sukhija, G. Kamath, M. Babshet, and H. S. Srikanth (2015). *IJSS Case Rep. Rev.* **2**, 36.
9. M. Gnanadesigan, M. Anand, S. Ravikumar, M. Maruthupandy, V. Vijayakumar, S. Selvam, M. Dhineshkumar, and A. K. Kumaraguru (2011). *Asian. Pac. J Trop. Med.* **4**, 799.
10. S. Iravani (2011). *Green. Chem.* **13**, 2638.

11. K. Kanagamani, P. Muthukrishnan, M. Ilayaraja, J. Vinothkumar, K. Shankar, and A. Kathiresan (2017). *J. Photochem. Photobiol. A.* **346**, 470.
12. G. Manjari, A. Parthiban, and S. Saran (2020). *J. Clust. Sci.* **31**, 1137.
13. N. Thirumagal and A. P. Jeyakumari (2020). *J. Clust. Sci.* **31**, 487.
14. K. Kanagamani, P. Muthukrishnan, K. Shankar, A. Kathiresan, H. Barabadi, and M. Saravanan (2019). *J. Clust. Sci.* **30**, 1415.
15. B. Thomas, B. Vithiya, T. Prasad, S. Mohamed, C. M. Magdalane, K. Kaviyarasu, and M. Maaza (2019). *J. Nanosci. Nanotechnol.* **19**, 2640.
16. A. Fouda, G. Abdel-Maksoud, M. A. Abdel-Rahman, S. S. Salem, S. El-Dinassan, and M. A. H. El-Sadany (2019). *Int. Biodeter. Biodegr.* **142**, 160.
17. S. W. P. Wijnhoven, W. J. G. M. Peijnenburg, C. A. Herberts, W. I. Hagens, A. G. Oomen, E. H. W. Heugens, B. Roszek, J. Bisschops, I. Gosens, D. V. E. Meent, S. Dekkers, W. H. De Jong, M. V. Zijverden, A. J. A. M. Sips, and R. E. Geertsma (2009). *Nanotoxicology* **3**, 109.
18. R. Langford and R. Burrell (1999). *J. Burn Care Rehabil.* **20**, 195.
19. V. Varadharaj, A. Ramaswamy, R. Sakthivel, R. Subbaiya, H. Barabadi, M. Chandrasekaran, and M. Saravanan (2020). *J. Clust. Sci.* **31**, 1257.
20. H. S. Rai, M. S. Bhattacharyya, J. Singh, T. K. Bansal, P. Vats, and U. C. Banerjee (2005). *Crit. Rev. Environ. Sci. Technol.* **35**, 219.
21. V. K. Gupta (2009). *J. Environ. Manage.* **90**, 2313.
22. B. Mokhlesi, J. B. Leikin, P. Murray, and T. C. Corbridge (2003). *Chest* **123**, 897.
23. M. S. Punnoose and B. Mathew (2018). *Mater. Sci. Eng.* **2**, 159.
24. M. Mavaei, A. Chahardoli, Y. Shokoohinia, A. Khoshroo, and A. Fattahi (2020). *Sci. Rep.* **10**, 1762.
25. S. K. Ahmed, W. B. Ali, and A. A. Khadom (2019). *Int. J. Ind. Chem.* **10**, 159.
26. D. K. Lavanya, F. V. Priya, and D. P. Vijaya (2020). *J. Fal. Anal. Prevs.* **20**, 494.
27. R. S. Nathiya, S. Perumal, M. Moorthy, V. Murugesan, R. Rangappan, and V. Raj (2020). *J. Bio. Tribo. Corros.* **6**, 1.
28. A. M. Abdel-Gaber, H. T. Rahal, and F. T. Beqai (2020). *Int. J. Ind. Chem.* **11**, 123.
29. P. Muthukrishnan, P. Prakash, K. Shankar, and A. Kathiresan (2018). *J. Fail. Anal. Prev.* **18**, 677.
30. W. Brand-Williams, M. E. Cuvelier, and C. Berset (1995). *Lebensm. Wiss. Technol.* **28**, 25.
31. Q. Liu, G. Zhu, and P. Huang (1991). *Zhongguo Zhong Yao Za Zhi* **16**, 50.
32. ASTM G 31 – 72, *Standard practice for labortary immersion corrosion testing of metals* (ASTM, West Conshohocken, PA, 1990).
33. M. A. Quraishi, M. A. W. Khan, M. Ajmal, S. Muralitharan, and S. V. Iyer (1997). *Corros. J.* **53**, 475.
34. P. Muthukrishnan, P. Prakash, M. Ilayaraja, B. Jeyaprabha, and K. Shankar (2015). *Metall. Mater. Trans. B* **46**, 1448.
35. S. M. Alsharif, S. S. Salem, M. A. Abdel-Rahman, A. Fouda, A. Mohamedid, S. H. El-Din, M. A. Awad, and A. A. Mohamed (2020). *Heliyon* **6**, 1.
36. K. A. Bogle, S. D. Dhole, and V. N. Bhoraskar (2006). *Nanotechnology* **17**, 3204.
37. A. M. Soliman, W. Abdel-Latif, I. H. Shehata, A. Fouda, A. M. Abdo, and Y. M. Ahmed (2020). *Bio Trace Elem Res*. https://doi.org/10.1007/s12011-020-02188-7.
38. M. Goudarzi, N. Mir, M. Mousavi-Kamazani, S. Bagheri, and M. Salavati-Niasari (2016). *Sci. Rep.* **6**, 1.
39. M. Nasrollahzadeh, S. M. Sajadi, F. Babaei, and M. Maham (2015). *J. Colloid Interf Sci.* **450**, 374.
40. A. Fouda, S. H. El-Din, A. M. Abdo, and M. S. El-Gamal (2020). *Bio Trace Elem. Res.* **195**, 707.
41. A. A. Mohmed, A. Fouda, M. S. Elgamal, S. H. El-Din, T. I. Shaheen, and S. S. Salem (2017). *Egypt J. Chem.* **60**, 63.
42. R. Vivek, R. Thangam, K. Muthuchelian, P. Gunasekaran, K. Kaveri, and S. Kannan (2012). *Process Biochem.* **47**, 2405.
43. A. Johnsona, I. Obota, and U. Ukponga (2014). *J. Mater. Environ. Sci.* **5**, 899.
44. Z. Yang and W. Zhai (2010). *Innov. Food. Sci. Emerg. Technol.* **11**, 169.
45. V. Kumar, D. Bano, S. Mohan, D. K. Singh, and S. H. Hasan (2016). *Mater. Lett.* **181**, 371.
46. J. C. Fantone and P. A. Ward (1982). *Am J Pathol.* **107**, 395.
47. F. Yang, X. Li, Z. Dai, T. Liu, W. Zheng, H. Zhao, and L. Wang (2017). *Int. J. Electrochem. Sci.* **12**, 7469.
48. Z. T. Khodair, A. A. Khadom, and H. A. Jasim (2019). *J. Mater. Res. Technol.* **8**, 424.
49. A. M. Atta, H. A. Allohedan, G. A. El Mahdy, and A. R. O. Ezzat (2013). *J. Nanomater.* **2013**, 1.
50. M. H. Mahmood, S. Suryanto, M. H. F. Al-Hazza, and F. I. Haidera (2018). *Int. J. Eng.* **31**, 450.
51. K. Parekh, S. Jauhari, and R. V. Upadhyay (2016). *Adv. Nat Sci. Nanosci Nanotechnol.* **7**, 1.
52. R. Najjar, A. M. A. Gaber, and R. Awad (2018). *Int. J. Electrochem. Sci.* **13**, 8723.
53. I. B. Obot, S. A. Umoren, and A. S. Johnson (2013). *J. Mater. Environ. Sci.* **4**, 1013.
54. A. S. Johnson, I. B. Obot, and U. S. Ukpong (2014). *J. Mater. Environ. Sci* **5**, 899.
55. J. Narenkumar, P. Parthipan, J. Madhavan, K. Murugan, S. Babu Marpu, A. K. Suresh, and A. Rajasekar (2018). *Environ. Sci. Pollut. Res.* **25**, 5412.
56. M. M. Solomon, H. Gerengi, S. A. Umoren, N. B. Essien, U. B. Essien, and E. Kaya (2018). *Carbohydr. Polym* **181**, 43.
57. K. Vignesh, R. Hariharan, M. Rajarajan, and A. Suganthi (2013). *Mater. Sci. Semicond. Process.* **16**, 1521.
58. R. Anjana and N. Geetha (2019). *IJSTR* **8**, 225.
59. A. A. Fairuzi, N. N. Bonnia, R. M. Akhir, M. A. Abrani, and H. M. Akil (2018). *IOB Conf. Ser. Earth Environ. Sci.* **105**, 1.
60. A. Miri, H. O. Shahraki Vahed, and M. Sarani (2018). *Res. Chem. Intermed.* **44**, 6907.
61. S. J. Joshi, S. J. Geetha, S. Al-Mamari, and A. Al-Azkawi (2018). *Jundishapur J. Nat. Pharm. Prod.* **13**, 1.
62. V. Kumar, R. Wadhwa, N. Kumar, and P. K. Maurya (2019). *3 Biotech* **7**, 1.
63. T. Akkini Devi, N. Ananthi, and T. P. Amaladhas (2016). *J. Nanostruct. Chem.* **6**, 75.